Response of granular material under combined principal stress value and orientation change in 3D space

Zhan He [a], Long Xue [a], Rui Wang [a] & Jian-Min Zhang [a]

[a] *Department of Hydraulic Engineering, State Key Laboratory of Hydroscience and Engineering, Tsinghua University.*

Abstract. Laboratory tests on soil adopt simplified stress paths compared to real world counterparts due to mechanical limitations. This study investigates the deformation of granular material under combined principal stress value and orientation change in full 3D space using the discrete element method. Such stress paths are achieved by applying a 3D force line boundary condition on spherical granular material samples. Continuous cyclic tests with stress paths restricted in a fixed plane and in full 3D space, simulating a bidirectional seismic stress path, are both conducted. The importance of taking both principal stress value and orientation change into consideration is highlighted. In the tests, the greatest deformation is observed under pure stress orientation change, while the smallest deformation is observed when the principal stress axes are fixed. The change of stress value and orientation in 3D is also shown to result in deformations different to those within a fixed plane. The origins of these differences are found to be associated with difference in shear modulus, dilatancy, and noncoaxiality at the macroscale, and particle contact and fabric anisotropy at the microscale.

Keywords. Granular material, DEM, principal stress value, principal stress orientation, 3D space

List of Symbols

D_{50}	The portions of particles with diameters smaller and larger than this value are 50%
D_{min}	Minimum particle diameter within the sample
D_{max}	Maximum particle diameter within the sample
r	Radius of the sample
σ_{ij}	Stress tensor
s_{ij}	Deviatoric stress tensor
$\sigma_{1,2,3}$	Deviatoric stress tensor
p	Mean effective stress
τ_{ij}	Shear stress at i direction, perpendicular to j direction
q	Deviatoric stress
q_{min}	Minimum deviatoric stress during simulation
q_{max}	Maximum deviatoric stress during simulation
ε_{ij}	Strain tensor
e_{ij}	Deviatoric strain tensor
ε_v	Volumetric strain
γ	Equivalent shear strain
F_{ij}	Deviatoric contact fabric tensor
G	Shear modulus
δ_{ij}	Kronecker delta
G	Shear modulus
I_m	Friction mobilization index
D	Dilatancy

1. Introduction

Soil is often subjected to 3D loading involving changes in both principal stress value and orientation under natural and engineering conditions. However, due to limitations in testing capability, the mechanical behaviour of soil is often evaluated under grossly simplified conditions, where the principal stress orientation is fixed in triaxial tests [Nakata et al., 1998] or rotated in a fixed plane in hollow cylinder torsional (HCT) shear tests [Arthur et al., 1980]. While these type of tests have provided valuable information for the advancement of soil mechanics, the representativeness of such an approach for real world 3D conditions needs to be assessed.

Existing studies have shown that the pure rotation of principal stress axes in a fixed plane perpendicular to the bedding plane of soil, as is in the hollow cylinder torsional shear test setup, can induce strains comparable to that under stress value change [Ishihara and Towhata, 1983; Ishihara and Yamazaki, 1984, 1980; Li et al., 2016; LI and YU, 2010; Miura et al., 1986a; Nakata et al., 1998; Tong et al., 2014; Towhata and Ishihara, 1985; Wang et al., 2019b; Xue et al., 2019; Yang et al., 2007]. This behaviour of soil has been attributed to the anisotropy of the material [Miura et al., 1986a]. Therefore, it can be naturally expected that stress paths combining principal stress value and orientation change in full 3D space would result in deformation different to those observed under relatively simple conditions.

Owing to mechanical limitations of test apparatuses, physical tests for such complex stress paths with principal stress value and orientation change are relatively scarce.

"2D stress paths" where the principal stress value and direction change simultaneously within a plane perpendicular to the bedding plane, following oval or "8"-shaped paths, have been achieved in the HCT apparatus [Ishihara and Yamazaki, 1980; Li, 1997; Towhata and Ishihara, 1985]. These test results clearly show that coupling stress orientation change with amplitude change can lead to greater deformation.

3D discrete element method (DEM) [Cundall and Strack, 1979] can provide an effective means to investigate the response of granular material under complex 3D loading, with the added convenience of allowing for the analysis of microscale quantities governing macroscale behaviour. Li et al. [2016] observed the contractive and non-coaxial strain of soil under continuous rotation of principal stress in 3D DEM. Sibille et al. [2019] simulated the response of sand under monotonic and cyclic nonproportional loading within the deviatoric stress plane (i.e., fixed principal stress axes, varying principal stress values and intermediate principal stress coefficient b values), to highlight the effectiveness of 3D DEM in quantitatively capturing the behaviour of sand under complex load paths. Several studies have been conducted using DEM to study the behaviour of soil under traffic loading, showing that the coupling of stress orientation change with value change can generate much greater deformation than under stress value change alone [Bian et al., 2020; Gu et al., 2020; Guo et al., 2022]. However, these analyses were only conducted for cases where the stress orientation change occurs within a fixed plane. Xue et al. [2019] proposed a "force line" boundary condition in 3D DEM to allow for the application of principal stress in any arbitrary direction. Using the method, Xue et al. [2019] conducted novel numerical tests where the principal stress axes rotation planes were oriented at different angles θ with respect to the bedding plane and showed that the change in stress orientation in 3D space has significant influence on the deformation of granular material.

The goal of this study is to investigate the deformation of granular material under combined principal stress value and orientation change in 3D space. The DEM method of Xue et al. [2019] was adopted. Numerical tests with the change of stress value and orientation within a fixed plane were first conducted and analysed to illustrate the influence of stress amplitude and orientation combined change on granular material response. Tests were then conducted to simulate the stress path generated under bidirectional shear wave induced ground shaking to assess the roles of stress principal stress value and orientation change for relatively realistic 3D loading.

2. Numerical Method

The DEM code used in this study was PFC3D [Itasca, 2018]. Spherical particles were used in the current study, where D_{50}=0.225mm D_{min}=0.115mm and D_{max}=0.305mm. Over 600,000 sphere particles were randomly generated and deposited under gravity, to achieve an anisotropic initial state. After deposition, a spherical sample of r = 3.6 mm, which contains approximately 21,540 particles (Fig. 1), is trimmed
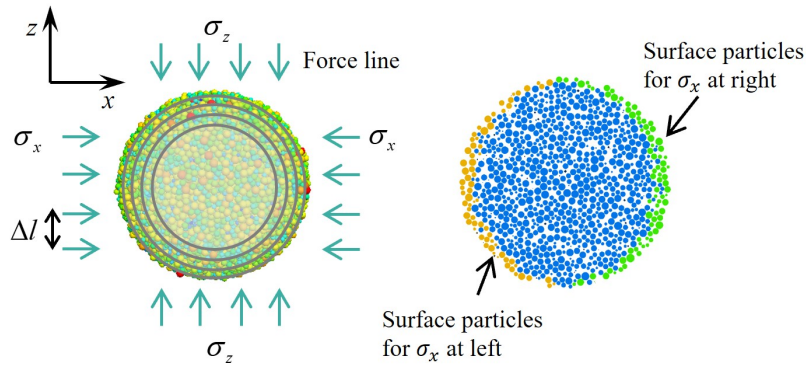
Figure 1. Schematic diagram of the sphere sample (21540 particles, e=0.686 0.689) and force line method for the application of stress. Note that the actual applied force line is much more densely distributed.

from the deposit. To examine the homogeneity of the sample, four spherical zones with different radius are selected to calculate the void ratio (Fig. 1). The void ratios of these four measure zones are consistent, ranging from 0.686 to 0.689. This sample is used for all simulation in the article. The sphere shape of the specimen is chosen for the convenience of the application of rotational principal stress boundary condition, and to reduce boundary effects that would otherwise be unavoidable for cubical shaped samples. The classic Hertz elastic contact model is used to characterize the particle contacts. The friction coefficient between particles is set to 0.5, damping is set to 0.2, Poisson's ratio is 0.15 while particle modulus is $2.5 \times 10^8 \text{N/m}^2$, which are selected based on existing studies [Jiang et al., 2020; Xue et al., 2019].

The desired stress boundary condition was applied on the spherical sample following the "force line" method proposed by Fu and Dafalias [2012] in 2D and Xue et al. [2019] in 3D. In this method, the target stress value is directly applied on the surface particles to allow for flexible control over stress direction, rather than on rigid walls, as is often done in DEM [Xue et al., 2019]. As illustrated conceptually in Fig. 1, force lines are uniformly distributed in three orthogonal directions at interval Δl, meaning that each force line is applied on the area Δl^2. Thus, the force value of each force line is $\sigma \Delta l^2$, where σ is the target principal stress value. This force is applied to the first particle that it comes into contact with as the line intersects the sample. The interval Δl was set to be smaller than the minimum particle radius to so that boundary particles are all constrained. Xue et al. [2019] showed that the method is effective in controlling the values and orientation of the principal stress freely in 3D space. For the numerical tests in this study, the sphere sample was first consolidated under isotropic stress conditions, and then loaded to the desired initial stress state. After that, the designated stress paths were applied on the sample. All tests are simulated under quasistatic conditions. The stress within a DEM sample can be expressed using the forces of particle contacts in the region as [Bagi, 1996]:

$$\sigma_{ij} = \frac{1}{V} \sum_{c \in V} f_i^c l_j^c \tag{1}$$

where σ_{ij} is the i, j component of the stress tensor over volume V. f_i^c is contact force at i direction. l_j^c is contact branch vector's j component. With the stress tensor, deviatoric stress q and mean effective stress p are calculated as:

$$p = \frac{\sigma_1 + \sigma_2 + \sigma_3}{3} \tag{2}$$

$$q = \sqrt{\frac{(\sigma_1 - \sigma_2)^2 + (\sigma_2 - \sigma_3)^2 + (\sigma_1 - \sigma_3)^2}{2}} \tag{3}$$

where $\sigma_{1,2,3}$ are the three principal stress values, from major to minor.

The determination of the strain of the entire sample can be obtained from an equivalent continuum corresponding to the granular sample [Bagi, 1996]. In a continuum, the average strain increment tensor expressed as Eq. (4), and Eq. (5) can be derived using Gauss' law:

$$d\overline{\varepsilon}_{ij} = \frac{1}{V} \int_V d\varepsilon_{ij} dV \tag{4}$$

$$d\overline{\varepsilon}_{ij} = \frac{1}{2V} \int_S (du_i n_j + du_j n_i) dS \tag{5}$$

where S is the surface area of the equivalent continuum and V is the volume of sample. du_i is the i component of the displacement vector and n_i is the i component of the unit vector which points outward from the surface. For a discrete system, the equivalent continuum can be generated as a convex hull of the Delaunay tessellation based on selected boundary particles [Xue et al., 2019], consisting of numerous triangles. Therefore, the average strain increment tensor can be expressed as Eq. (6) [Xue et al., 2019]:

$$d\overline{\varepsilon}_{ij} = \frac{1}{2V} \sum_{k=1}^{N_t} (du_i^k n_j^k + du_j^k n_i^k) S^k \tag{6}$$

where N_t is the number of triangles on the convex hull. $d\vec{u}^k$ and $\vec{n}^k$ are the displacement vector and the outward normal unit vector of the kth triangle, respectively. S^k is the area of kth triangle.

The deviatoric strain tensor e_{ij} can be calculated from the strain tensor ε_{ij}:

Open Geomechanics, 2022, article no. 4

Zhan He, Long Xue, Rui Wang & Jian-Min Zhang, *Response of granular material under combined principal stress value and orientation change in 3D space*

3

$$e_{ij} = \varepsilon_{ij} - \frac{1}{3}\varepsilon_{kk}\delta_{ij} \qquad (7)$$

The equivalent shear strain can thus be defined as:

$$\gamma = \sqrt{\frac{2}{3}\sum_{i=1}^{3}\sum_{j=1}^{3}e_{ij}e_{ij}} \qquad (8)$$

Considering the sphere particles, the contact normal fabric tensor is used to describe the anisotropy of the sample, defined as [Satake, 1982]:

$$F_{ij} = \frac{1}{N}\sum_{k=1}^{N} v_i^k v_j^k - \frac{1}{3}\delta_{ij} \qquad (9)$$

where F_{ij} is the i, j component of the average deviatoric contact fabric tensor over contact number N. v_i is the i component of unit contact vector. δ_{ij} is the Kronecker delta. The initial anisotropic state of the sample is also measured through Eq. (9):

$$F_0 = \begin{bmatrix} -0.00943 & 0.00118 & -0.00248 \\ 0.00118 & -0.00653 & 0.00083 \\ -0.00248 & 0.00083 & 0.01587 \end{bmatrix} \qquad (10)$$

where F_{zz}=0.01587, obviously larger than F_{xx} and F_{yy}, implying that the dominant direction of contact is close to z direction (gravity direction).

3. Stress value and orientation change within a fixed plane

3.1. Stress path

The response of granular material under three types of idealized stress paths where the principal value or/and orientation change within a fixed plane is first investigated. 7 tests are conducted, as shown in Table 1, where q_{min} and q_{max} are the minimum and the maximum deviatoric stress during test, respectively. Three types of stress paths are applied, namely "straight-line", "circular", and "8-shaped". The stress paths are visualized in Fig. 2 in both $\tau - \sigma$ space and in 3D space, where the green lines represent the trajectory of the major principal stress, the $x - y$ plane is the bedding plane of the sample, and the z axis is perpendicular to it. The samples are first isotropically consolidated to a mean stress p of 100 kPa for all stress paths. The major principal stress vector follows such a sequence of S1-S2-S3-S4-S1 in all tests.

Under the straight-line stress path, only principal stress value change is applied, where σ_2 is kept constant as the intermediate principal stress in the y direction and the other two principal stresses remain in the $x - z$ plane (Fig. 2 (a)). During cyclic loading after consolidation, in the first half cycle, the angle between σ_1 and the positive x direction is 45°, and σ_1 increases until deviatoric stress q reaches the peak value at 1/4 cycle (S2) and then decreases until q is 0 kPa at half cycle (S3). In the second half cycle, σ_1 transitions to be perpendicular to its previous orientation, at an angle of 135° with respect to the positive x direction. This stress path is consistent with that of cyclic shearing within the bedding plane after isotropic consolidation.

In the case of circular stress path, only stress axes orientation change occurs, without any principal stress value change (Fig. 2 (b)). After isotropic consolidation, the deviatoric stress q is increased to 30 kPa or 50 kPa according to Table 1, under constant p, where σ_3 is in the x direction, σ_2 is in the y direction, and σ_1 is in the z direction. During circular stress path loading, the principal stress values are then kept constant and one of the principal stress axis is fixed while the other two rotate around it clockwise continuously.
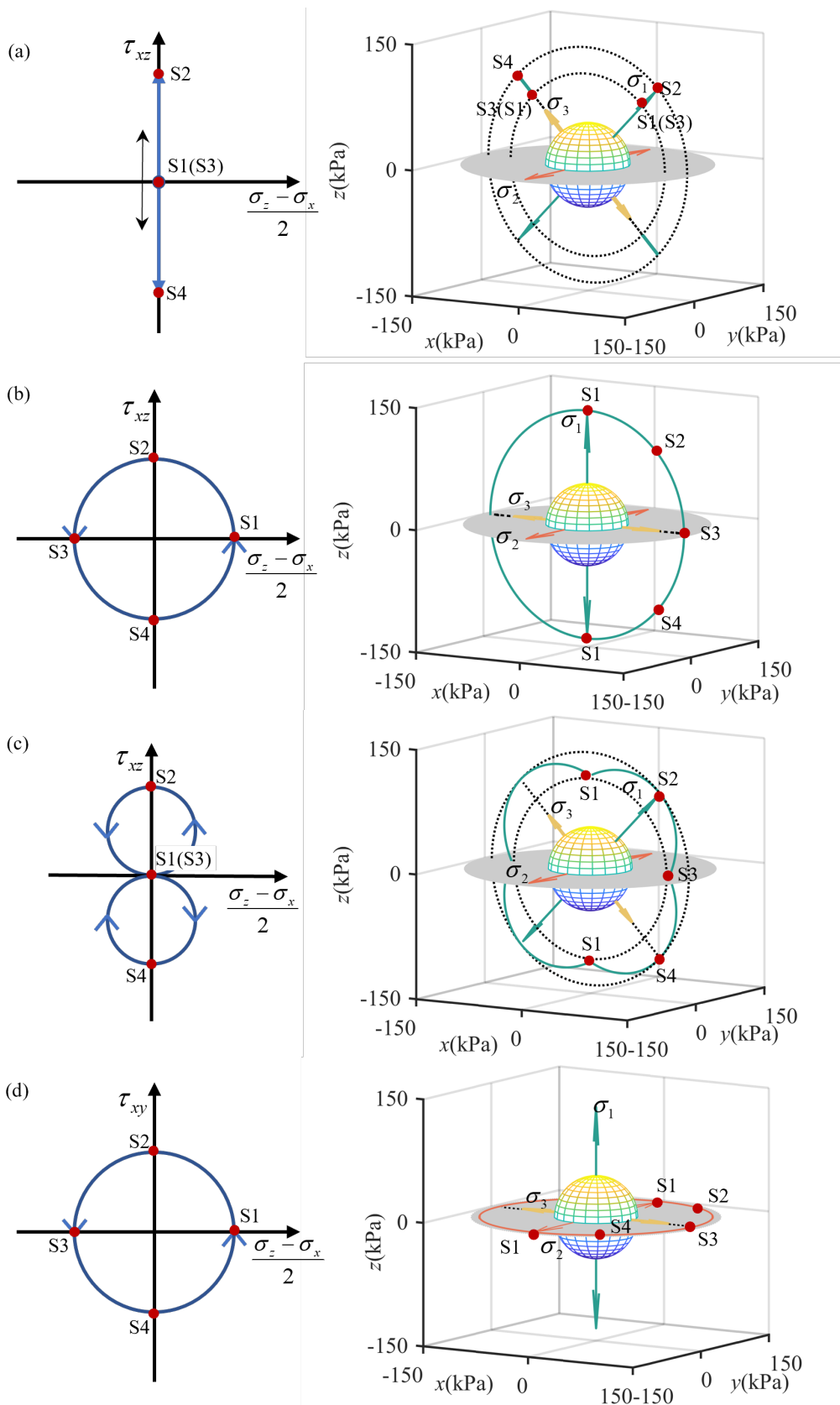
In order to investigate the joint effect of principal stress value and orientation change, the "8"-shaped stress path is designed where both principal stress value and orientation change occur (Fig. 2 (c)). This type of loading initiates from the consolidated isotropic stress state, and σ_1 increases during the first 1/4 cycle as σ_1 and σ_3 rotate around σ_2 clockwise, resulting in increased deviatoric stress q while p remains constant. After q reaches its peak value at 1/4 cycle, and σ_1 decreases until q is 0 kPa at 1/2 cycle. This is repeated during the second half cycle, and then on for further cycles.

For test series 1 and 2 in Table 1, the change in principal stress value and orientation only occurs within the $x - z$ plane, as shown in Fig. 2 (a), (b), and (c). For comparison, test HS-50-50-R where the principal stress axes are rotated within the $x - y$ plane is also conducted (Fig. 2 (d)). In all simulations, the mean stress remains 100 kPa, while the peak deviatoric stress q_{max} is 30 kPa and 50 kPa in series 1 and 2, respectively.

3.2. Deformation

The volumetric strain development for the tests in Table 1 are illustrated in Fig. 3. Continuous contractive (positive) volumetric strain is observed for all the stress paths, while oscillations are also observed within each cycle. The most significant volumetric strain accumulation occurs within the first several load cycles, with the volumetric strain within the first three cycles accounting for more than 40% of that after 30 load cycles in all cases. Such accumulation would slow down and the volumetric strain would reach an asymptotic state [Wang et al., 2019b; Xue et al., 2019]. Although the amplitude of deviatoric stress value change is the same for the three types of stress paths in series 1 and 2, respectively, distinctly different volumetric strain is observed. The volumetric strain under the straight-line stress path with only principal stress value change is the smallest (L-0-30-F and L-0-50-F), while that under the circular stress path with only principal stress orientation change is the greatest (S-30-30-R and S-50-50-R). The volumetric strain of L-0-30-F is comparable with the tests of Wichtmann and Knittel [Wichtmann and Knittel, 2020]. Interestingly, the volumetric strain under the "8"-shaped stress path with both principal stress value and orientation change is between the other two. These results agree qualitatively with the undrained cyclic torsional tests by Towhata and Ishihara [1985], which showed that the liquefaction resistance of sand under a half- "8"-shaped stress path is lower than straight-line stress path. Also, comparison between the results of series 1 and 2 show that greater deviatoric stress amplitude produces

Open Geomechanics, 2022, article no. 4
Zhan He, Long Xue, Rui Wang & Jian-Min Zhang, *Response of granular material under combined principal stress value and orientation change in 3D space*

4

Figure 2. Stress paths for tests of stress value and orientation change within a fixed plane: (a) Straight-line; (b) Circular; (c) "8"-shaped; (d) Circular (Horizontal).

greater volumetric deformation under the same type of stress path. For L-0-30-F and S-30-30-R, owing to small shear stress ratio, there is very little plastic volumetric strain accumulation for L-0-30-F and more plastic deformation is

Table 1. Numerical simulations.

Test series	Test ID	Stress path type	q_{min} (kPa)	q_{max} (kPa)	p (kPa)
1	L-0-30-F	Straight-line	0	30	100
	S-30-30-R	Circular	30	30	100
	B-0-30-R	"8"-shaped	0	30	100
2	L-0-50-F	Straight-line	0	50	100
	S-50-50-R	Circular	50	50	100
	B-0-50-R	"8"-shaped	0	50	100
3	HS-50-50-R	Circular (Horizontal)	50	50	100
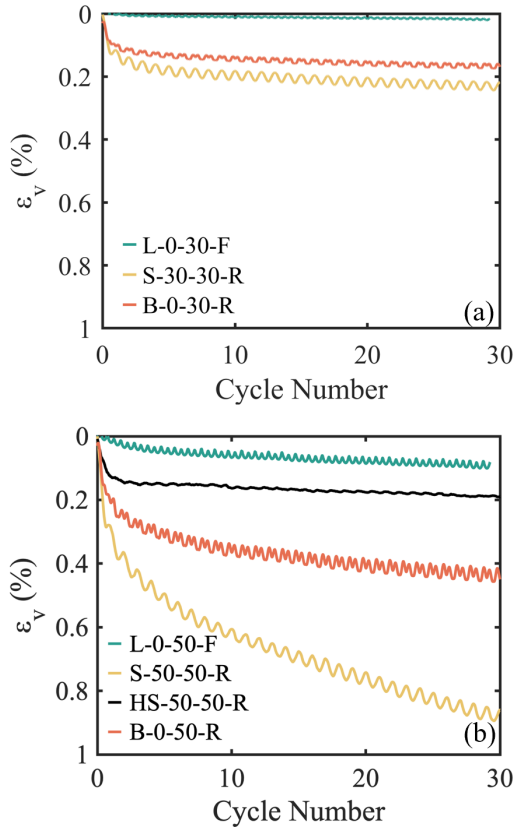
Figure 3. Volumetric strain for tests of stress value and orientation change within a fixed plane: (a) series 1; (b) series 2 and 3.

induced under principal stress orientation change, resulting in large difference between L-0-30-F and S-30-30-R. When the shear stress ratio increases, the plastic strain of the sample significantly increases for the fixed stress orientation loading case(L-0-50-F), resulting in smaller difference between L-0-50-F and S-50-50-R. It shows that the stress amplitude is also an important influence factor.

The volumetric strain of S-50-50-R and HS-50-50-R can be compared in Fig. 3 (b). The difference between the two tests is the different principal stress orientation rotation in 3D space. The sample is more easily to be compressed when the major principal stress is rotated to horizontal plane, which is achieved in S-50-50-R. When the major principal stress is in the vertical direction, the sample is more difficult to be compressed, in HS-50-50-R. Therefore, the

volumetric strain under S-50-50-R is much greater than that of HS-50-50-R.

Fig. 4 plots the equivalent shear strain of all tests. Shear strain also accumulates with continuous loading, yet with stronger oscillation than that of the volumetric strain during each cycle. Similar to the volumetric strain, the greatest shear strain is observed under the circular stress path, while the smallest is observed for the straight-line stress path. Greater deviatoric stress leads to greater deviatoric strain under the same type of stress path. Similar to volumetric strain, the plastic sliding is triggered with greater deviatoric stress amplitude, resulting in larger plastic deformation accumulation. Fig. 4 (b) also shows that the shear strain under S-50-50-R is much greater than that of HS-50-50-R, following the same pattern as that of the volumetric strain.

These results show that the change in principal stress orientation coupled with principal stress value change can significantly affect the deformation of granular materials. Also, the comparison between series 3 and 2 indicates that the deformation of granular material under stress paths in 3D space can be rather different to that of idealized fixed plane or 2D cases. Owing to anisotropy of the deposited sample, shear can occur more easily within the deposit bed. Thus, greater deformation is observed under S-50-50-R.

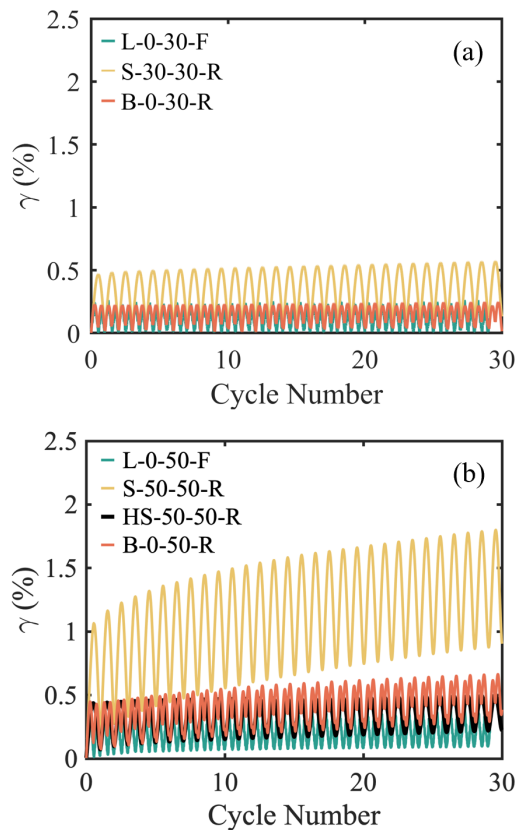## 3.3. Macroscale and microscale causes for the difference in deformation

In order to reveal the reason for different deformation patterns observed for the different types of loading, the shear modulus and dilatancy under the four types of stress paths are evaluated, along with some contact-based microscale quantities. The shear modulus is defined as:

$$G = \frac{\sqrt{\sum_{i=1}^{3}\sum_{j=1}^{3}\mathrm{d}s_{ij}\mathrm{d}s_{ij}}}{2\sqrt{\sum_{i=1}^{3}\sum_{j=1}^{3}\mathrm{d}e_{ij}\mathrm{d}e_{ij}}} \quad (11)$$

where $\mathrm{d}s_{ij}$ is the increment of deviatoric stress tensor s_{ij}, obtained from stress tensor:

$$s_{ij} = \sigma_{ij} - \frac{1}{3}\sigma_{kk}\delta_{ij} \quad (12)$$

Fig. 5 shows the evolution of shear modulus for the three test series. The comparison of shear modulus between the various tests agrees with that of the shear strain in Fig. 5, as one would expect. The shear modulus oscillates within each

Open Geomechanics, 2022, article no. 4

Zhan He, Long Xue, Rui Wang & Jian-Min Zhang, *Response of granular material under combined principal stress value and orientation change in 3D space*

6

Figure 4. Shear strain for tests of stress value and orientation change within a fixed plane: (a) series 1; (b) series 2 and series 3.
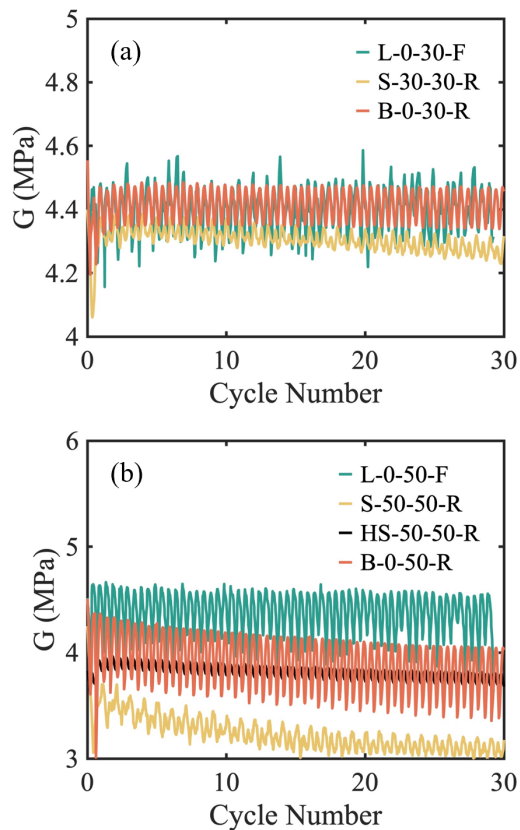
Figure 5. Shear modulus for tests of stress value and orientation change within a fixed plane: (a) series 1; (b) series 2 and 3
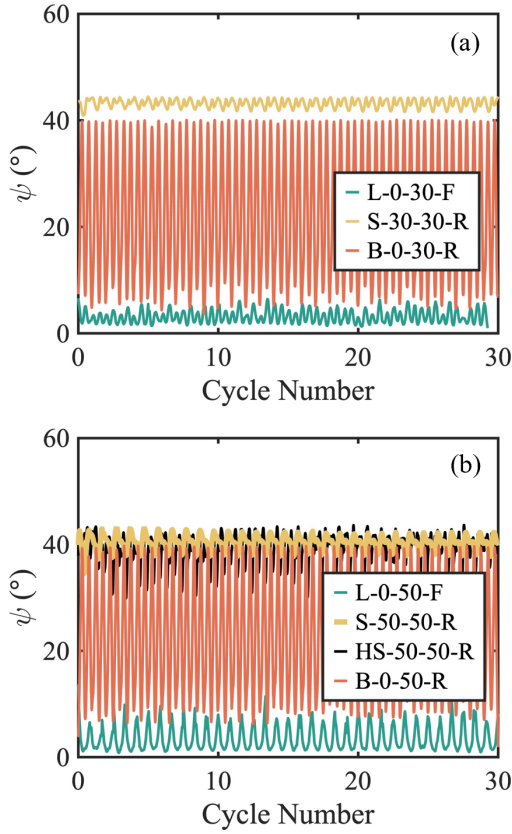
load cycle, and there is also generally a trend of decrease to reach a stable value in shear modulus as the loading advances, which is more obvious for the tests with greater deviatoric stress amplitude, i.e., series 2. The samples that undergo circular stress path in the vertical plane (S tests) exhibit the lowest shear modulus, resulting in the greatest deviatoric strain, while the samples subjected to the straight-line stress path exhibit the highest shear modulus, corresponding to the smallest deviatoric strain in Fig. 5. Test HS-50-50-R yields higher shear modulus than S-50-50-R (Fig. 5 (b)), resulting in the smaller shear deformation in Fig.4.

The non-coaxial phenomenon, which refers to the non-coaxiality between strain increment and stress, is an important observation when principal stress orientation change occurs [Ishihara and Towhata, 1983], and has often been considered to be a major contributor to the deformation of granular materials under such loading conditions [Wu et al., 2021]. Here, the definition of non-coaxial angle ψ is used as the relative orientation of major principal eigenvector of stress and major principal eigenvector of strain increment within the plane generated by major principal eigenvector of stress increment and major principal eigenvector of strain increment. The greatest ψ is observed for the circular stress path in the vertical plane, and that of the "8"-shaped stress path comes in between the circular stress path and the straight-line stress path, which follows the same pattern

as deformation in Fig. 3 and Fig. 4 and is opposite to the pattern of shear modulus in Fig. 5. In S-30-30-R, the deviatoric stress is constant at q = 30 kPa while the orientation of the principal stress changes, and non-coaxial angle shows small oscillations around 42°, and reaches its peak when major principal stress is rotated to the horizontal plane. However, In B-0-30-R, the deviatoric stress value changes as the principal stress orientation changes, resulting in violent fluctuation of non-coaxial angle. When the major principal stress is rotated to the horizontal plane, the deviatoric stress is 0 kPa, resulting in a small non-coaxial angle. For circular stress path in the horizontal plane, HS-50-50-R yields smaller ψ than S-50-50-R. This suggests that, for the same sample under different stress paths with the same deviatoric stress amplitude, the shear modulus and deformation of the material is strongly associated with the non-coaxial angle between strain increment and stress.

On the microscale, the mobilized interparticle friction is a factor that would be directly associated with the shear deformation and modulus of the granular material. Here, a friction mobilization index is used to quantify the contact sliding conditions:

$$I_m = \frac{|f_t|}{\mu_t f_n} \tag{13}$$

Open Geomechanics, 2022, article no. 4
Zhan He, Long Xue, Rui Wang & Jian-Min Zhang, *Response of granular material under combined principal stress value and orientation change in 3D space*

7

Figure 6. Non-coaxial angle for tests of stress value and orientation change within a fixed plane: (a) series 1; (b) series 2 and 3
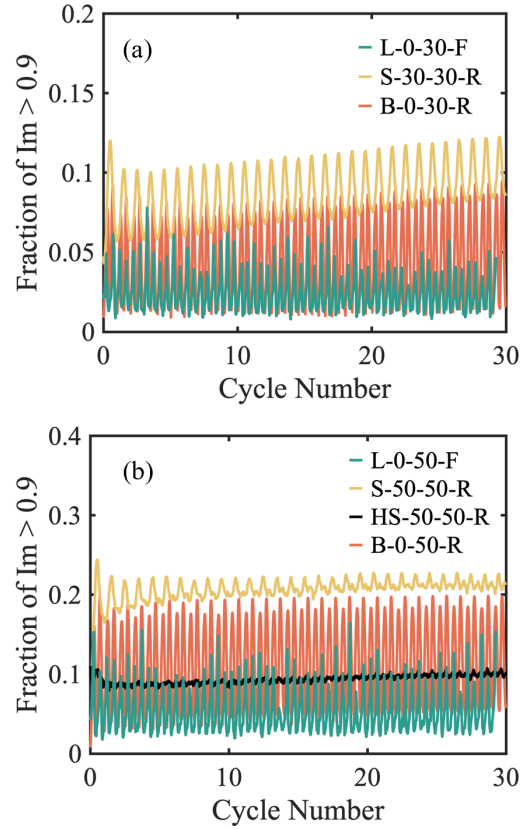
Figure 7. Fraction of contacts where $I_m > 0.9$ for tests of stress value and orientation change within a fixed plane: (a) series 1; (b) series 2 and series 3

where μ_t is the friction coefficient between two particles, f_t is the tangential contact force and f_n is the normal contact force. $I_m = 1$ indicates sliding contact. Fig. 7 shows the fraction of contacts where the friction mobilization index is large than 0.9 for all of the tests, which indicates the percentage of contacts that are sliding or close to sliding. It can be observed that more contact sliding is mobilized under circular path compared to the other two stress paths, resulting in smaller shear modulus and larger deformation, while the least contact sliding occurs for the straight-line stress path. For test series 3, under HS-50-50-R stress path, fewer contacts are mobilized than S-50-50-R, leading to higher shear modulus.

These analyses indicate that as stress orientation and value change, the mobilized friction within the contacts can change significantly at the microscale, resulting in the macroscale phenomenon of non-coaxiality and thus affect the shear modulus and shear deformation of granular material.

As the mean effective stress remains unchanged in all of the tests, the volumetric strain is caused by the dilatancy of granular material, which refers to the volumetric strain generated via shear, quantified as:
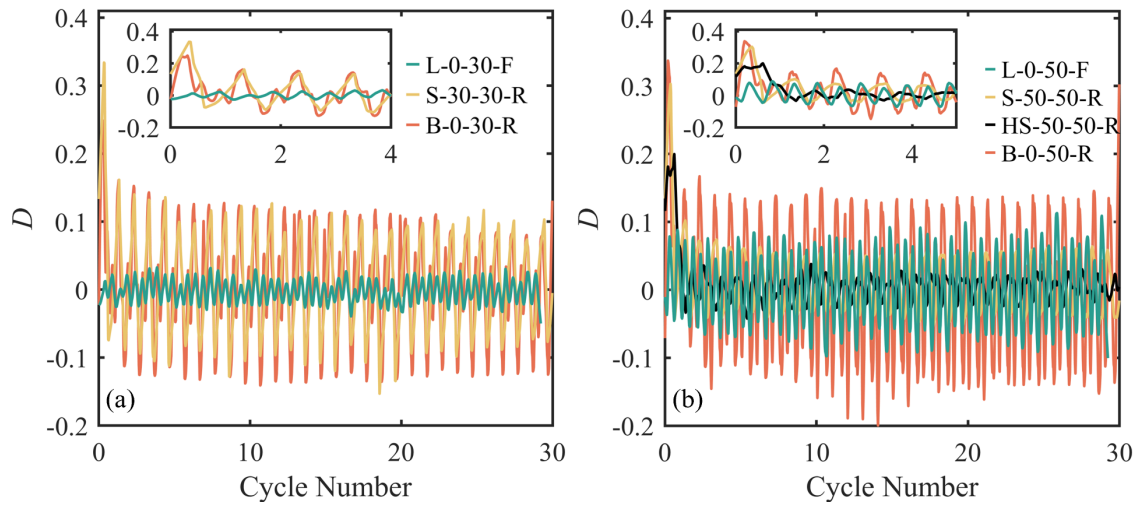
$$D = \frac{\Delta\varepsilon_v}{\Delta\gamma} \qquad (14)$$

Fig. 8 shows the dilatancy under the three kinds of stress paths for the first ten load cycles. During the first two load cycles, relatively strong positive dilatancy (positive refers to contraction) is observed under the circular and "8"-shaped stress paths, whereas the initial positive dilatancy is not as strong under the straight-line stress path. The dilatancy in the first load cycles of series 2 is greater than that of series 1, as greater deviatoric stress amplitude is applied. Also, for HS-50-50-R stress path, during the first several cycles, the positive dilatancy is smaller than S-50-50-R, causing smaller volumetric deformation. After 2-3 load cycles, dilatancy begins to oscillate around zero for all the stress paths, agreeing with observations in Fig. 3 that volumetric strain stabilizes after a few load cycles.

The difference in dilatancy for the three types of stress paths lies within the influence of anisotropy [Miura et al., 1986b]. Wang et al. [2019a] showed that the relative orientation between loading and fabric anisotropy can significantly affect the dilatancy of granular material, triaxial tests on samples with greater bedding plane angles yielded greater initial positive dilatancy. To assess the influence of fabric anisotropy, Initial Fabric Anisotropy Variable A is used to quantify the relative angle between the deviatoric strain increment tensor and initial contact normal fabric tensor:

$$A = \mathrm{d}e_{ij}F_{ij}^0 \qquad (15)$$

Open Geomechanics, 2022, article no. 4
Zhan He, Long Xue, Rui Wang & Jian-Min Zhang, *Response of granular material under combined principal stress value and orientation change in 3D space*

8

Figure 8. Dilatancy for tests of stress value and orientation change within a fixed plane: (a) series 1; (b) series 2 and series 3

where de_{ij} and F_{ij}^0 are the deviatoric strain increment tensor and initial contact normal fabric tensor, respectively. Positive A generally means that the deviatoric strain increment is more aligned with initial contact normal fabric. Here, the initial fabric tensor is used rather than the current fabric tensor because when the stress rotates within the bedding plane for the HS-50-50-R test, the weak initial anisotropy within the bedding plane would easily evolve under such stress path, affecting the interpretation of the data.

Fig. 9 shows the scatter plot of dilatancy against A at the 1st, 10th and 20th cycle for the three different types of stress paths, along with the linear fit of the first cycle. It shows that there is generally more contraction tendency when A has a greater negative value. The linear fit between D and A are also plotted in Fig. 9, with the slope of the D-A fit being negative for all the cases, except for L-0-50-F, where A remained almost constant. These findings are in agreement with existing studies on stress paths with only principal stress value change [Wang et al., 2019a]. It is worth pointing out that the variation range of A under straight-line stress path is much smaller than that in the other two cases and oscillates at approximately zero even at the very beginning, resulting in near symmetrical dilatancy with respect to zero, and sign of the slope of the linear fit is not very meaningful. When principal stress orientation change is included, the variation range of A is expanded, D tends to be greater for negative A under the circular and "8"-shaped stress paths, indicating more contraction. This asymmetrical dilatancy development due to anisotropy significantly affects volumetric strain accumulation. Although the dilatancy under the circular and "8"-shaped stress paths are similar quantitatively, the accumulated volumetric strain is greater under the circular stress path due to the smaller shear modulus and greater shear strain. For HS-50-50-R, the variation range of A is also limited compared to S-50-50-R, resulting smaller initial volumetric contraction. This shows that fabric

anisotropy plays a significant role in the dilatancy and volumetric deformation of granular material, especially when stress orientation change occurs along with value change.

4. Seismic Stress Path Simulation

4.1. Bidirectional seismic stress paths

Reality often yields even more complex stress paths in 3D space than those discussed in the previous section, where stress value and orientation change within a fixed plane. One typical case is seismic stress path. Cyclic shear loads of two horizontal directions is often induced at the same time in soil during earthquakes, as reported by several studies [Ishihara and Yamazaki, 1980; Li, 1997; Zeghal et al., 2018]. This can result in stress states similar to that shown in Fig. 10 (a). As the two shear stress components change independently, the orientation of stress changes in 3D space accompanied by stress value change, and would be expected to affect soil deformation according to the analysis in the previous section. Here, a simplified bidirectional seismic stress path acting on a soil element is represented by:

$$\begin{bmatrix} \sigma_x & \tau_{xy} & \tau_{xz} \\ \tau_{xy} & \sigma_y & \tau_{yz} \\ \tau_{xz} & \tau_{yz} & \sigma_z \end{bmatrix} = \begin{bmatrix} p_0 & 0 & \tau_1\cos\omega \\ 0 & p_0 & \tau_2\sin\omega \\ \tau_1\cos\omega & \tau_2\sin\omega & p_0 \end{bmatrix} \quad (16)$$

For comparison, three other types of stress paths are also simulated in companion to the stress path of test D-B, including pure principal stress value change test D-F, pure 3D principal stress orientation change test D-R and pure principal stress orientation with respect to σ_2 test D-R2, visualized in Fig. 10 (d)~(f). These tests follow stress paths that are simplified from that of test D-B to identify the roles of principal stress value and orientation changes in 3D space. In test D-F (Fig. 10 (d)), only the principal stress value change that occurs in test D-B is applied, without any principal stress orientation. In test D-R (Fig. 10 (e)), the principal stress value is kept constant as initial state of test
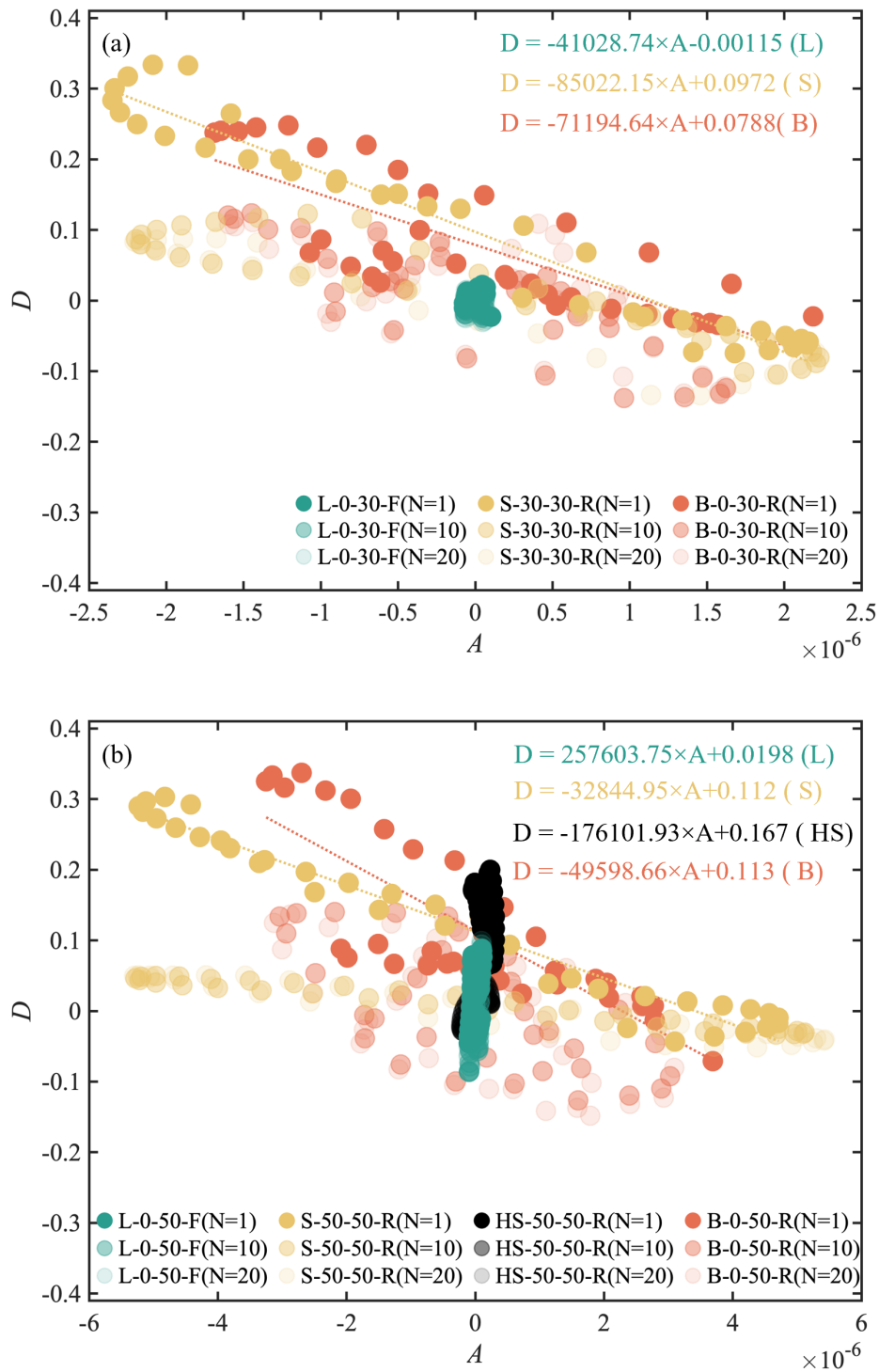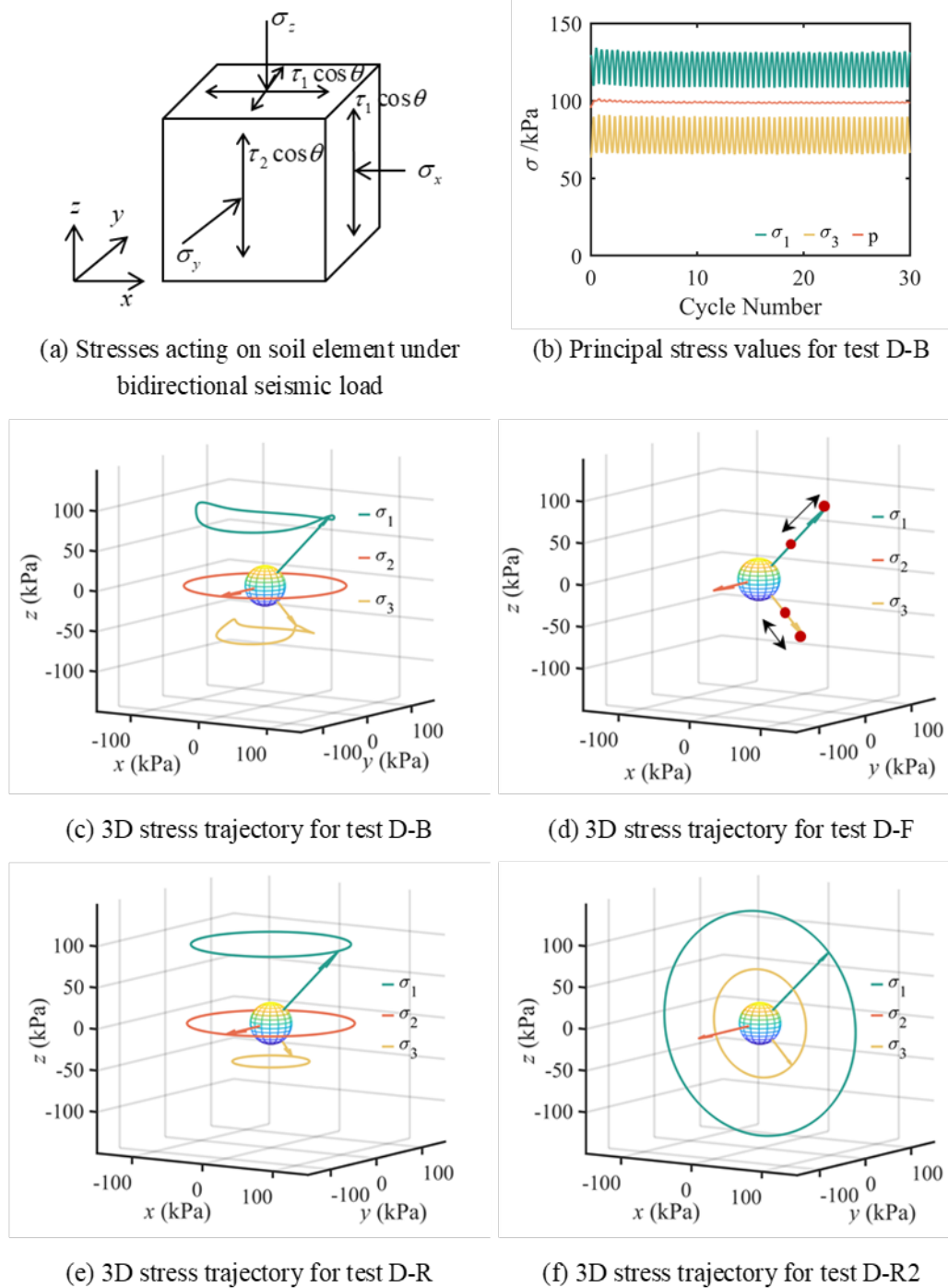
Figure 9. Scatter plot of dilatancy versus A at 1st, 10th, 20th cycle for tests of stress value and orientation change within a fixed plane: (a) series 1; (b) series 2 and series 3. The linear fit between dilatancy D and the initial fabric anisotropy variable A for the first load cycle is also plotted for reference.

D-B, while principal stress orientation change follows that of test D-B. In test D-R2 (Fig. 10 (f)), principal stress orientation change is restricted to the plane perpendicular to σ_2, as a comparison to real 3D stress rotation, while the principal stress value is kept constant as D-R. Also, quasistatic simulations are conducted here instead of the real time dependent

dynamic process of earthquakes to focus on the combined effect of principal stress value and direction change.

4.2. Deformation

The volumetric strain development for the tests in Fig. 10 is illustrated in Fig. 11 (a). Similar to the situation in the tests

(a) Stresses acting on soil element under bidirectional seismic load

(b) Principal stress values for test D-B

(c) 3D stress trajectory for test D-B

(d) 3D stress trajectory for test D-F

(e) 3D stress trajectory for test D-R

(f) 3D stress trajectory for test D-R2

Figure 10. Stress paths for bidirectional seismic stress path tests, including bidirectional seismic stress path test D-B, pure principal stress value change test D-F, pure 3D principal stress orientation change test D-R, and pure principal stress orientation with respect to σ_2 test D-R2.

stress value and orientation change within a fixed plane, continuous contractive (positive) volumetric strain is observed with oscillations during each cycle. Most volumetric accumulation occurs within the first several load cycles and eventually the accumulation would slow down resulting in stable volumetric strain. For the D-B, D-F, and D-R tests, the smallest volumetric strain occurs in D-F with only principal stress value change, while the most pronounced volumetric contraction is observed in D-R with only principal stress orientation change. This is consistent with the observations in the previous section for stress paths within fixed planes. For D-R and D-R2, slightly larger volumetric deformation occurs in D-R2.

Fig. 11 (b) plots the equivalent shear strain of the tests. Strong shear strain oscillation is observed within each cycle with the greatest amplitude during the first few load cycles,

(a) Volumetric strain

(b) Equivalent shear strain
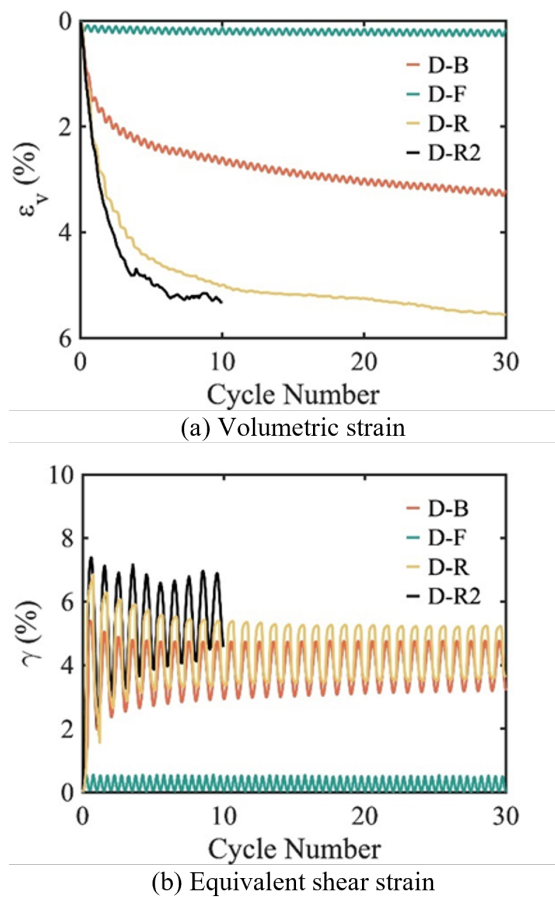
Figure 11. Volumetric strain and shear strain of the seismic load simulation stress paths tests D-B, D-F, D-R, and D-R2.

which then reduces gradually to reach a stable level. Rapid development of shear strain is observed within the first load cycle, especially in tests D-B and D-R, and then shear strain reaches an overall stable level, which is different to the slow accumulation of shear strain in Fig. 4. The strain under test D-B is between pure 3D principal stress orientation change test D-R and stress value change test D-F, similar to the tests of stress paths within fixed planes. In D-R2, the shear strain is slightly larger than D-R during the first few load cycles.

The difference in deformation among tests D-B, D-F, and D-R further shows that both the change in principal stress orientation and principal stress value change can affect the response of granular material in 3D space, with patterns similar to those for the stress paths within a fixed plane. On the other hand, the difference between D-R and D-R2 suggests that the deformation is also affected by whether the principal stress is rotated freely in 3D or in a fixed plane.

4.3. Macroscale and microscale causes for the difference in deformation

To better understand the cause of the deformation in the 3D tests, the shear modulus and dilatancy, along with microscale parameters, are evaluated. Fig. 12 (a) shows the evolution of shear modulus for the tests. There is a rapid

drop of shear modulus within the first load cycle followed by gradual increase again. The rapid drop of shear modulus in the first load cycle matches the observation of rapid shear strain development in Fig. 11 (b), while the later gradual increase in shear modulus explains the gradual decrease in shear strain oscillation amplitude. Corresponding to shear strain, the lowest equivalent shear modulus is observed in D-R test with pure principal stress orientation change, while the highest is observed in D-F. This is associated with non-coaxiality and contact sliding. As shown in Fig. 12 (b) and (c), most contacts would be mobilized in D-R stress path with the greatest non-coaxial angle, while the smallest under D-F stress path. As for D-R and D-R2, similar contact sliding can be observed, resulting in similar non-coaxial angle and shear modulus, especially during first few cycles. These results show once more that a greater non-coaxial angle is associated with more mobilized contacts, which would generate a lower equivalent shear modulus, resulting in more significant shear strain.

Fig. 12 (d) shows the dilatancy for the 3D tests. During first few cycles, only positive dilatancy is achieved under D-B, D-R and D-R2 stress paths, which leads to the significant volumetric contraction in Fig. 11 (a). Dilatancy under D-F stress path is mostly oscillatory, leading to small volumetric strain accumulation. After 10 cycles, dilatancy oscillates around zero for all tests, resulting in stabilized volumetric strain values. Even though larger dilatancy is observed for D-B than D-R, greater volumetric contraction occurs in D-R due to smaller shear modulus and greater shear strain (Fig. 11(b) and Fig. 12(a)). Slightly smaller dilatancy is observed for D-R2 compared with D-R. However, the slightly lager shear strain in D-R2 results in larger volumetric deformation.

Fig. 13 shows the scatter plot of dilatancy against initial fabric anisotropy variable A at the 1st, 10th cycle for the 3D tests and also the linear fit between D and A for the first cycle. For all four stress paths, D is negatively affected by A during the first load cycle. The variation range of A is limited for D-F stress path, similar to the case of fixed stress orientation in Fig. 9, the sample experiences mostly oscillating dilatancy and volumetric strain. As for the other three stress paths, smaller value of A is achieved as the orientation of stress changes, resulting in enhanced contraction and subsequent accumulation of positive volumetric strain, similar to the situation when principal stress is within a fixed plane.

According to the analysis from seismic load simulations, the effect of principal stress value and orientation change is highlighted again, and also emphasizes the need to consider the changes in 3D space when assessing the behaviour of granular material under realistic loading conditions.

5. Conclusions

DEM is used in this study to investigate the behaviour of granular materials under complex 3D stress paths. Realistic stress paths where the stress orientation and values vary freely in 3D space is achieved for the first time, using the force line method to realize arbitrary stress boundary conditions.
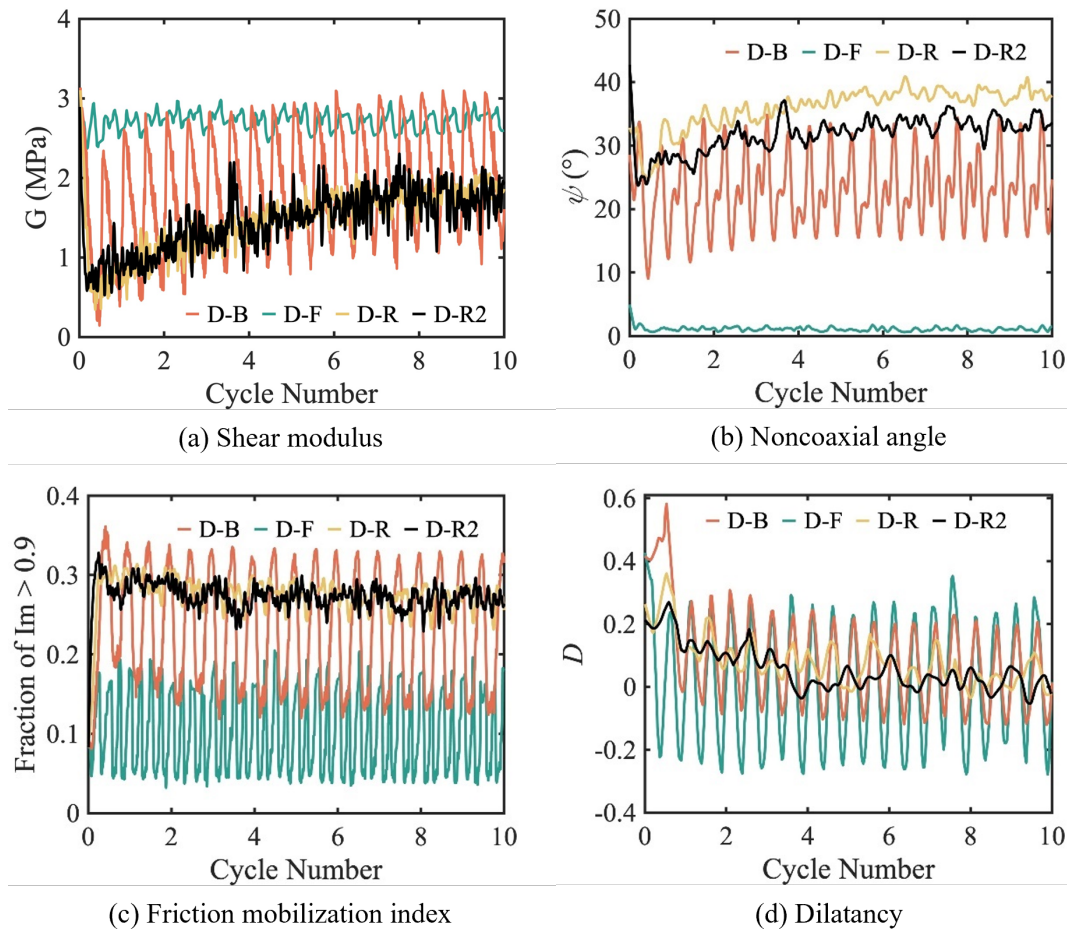
Figure 12. Shear modulus, non-coaxial angle, friction mobilization index and dilatancy of the seismic load simulation stress paths tests D-B, D-F, D-R, and D-R2.

Under continuous cyclic stress paths within a given fixed plane, granular material is observed to experience continuous volumetric contraction and shear strain accumulation. The greatest deformation is observed under circular stress path where the orientation of stress changes while the principal values remain constant. The deformation under straight-line stress path with only principal stress value change exhibits the smallest deformation. Corresponding to shear strain, the shear modulus reduces when principal stress orientation change is included, which can be associated with increased contact sliding and non-coaxiality. Under the same loading conditions, D tends to be greater for negative A, and vice versa, indicating that fabric anisotropy plays a major role in the dilatancy, and subsequently volumetric deformation, of granular material under the combined effect of principal stress value and orientation change.

For real 3D stress paths, a bidirectional seismic load simulation is conducted along with its variants for comparison. Similar patterns of influence by stress orientation change on non-coaxiality, contact sliding, shear modulus and shear strain is observed, as those in stress paths within a fixed plane. The relationship between D and A becomes more complex, but still generally shows that D tends to

be negatively affected by A. This results in asymmetrical development of D for stress paths that incorporate stress orientation change, causing the rapid accumulation of volumetric strain within the first few load cycles. The results indicate the necessity to consider the change of stress orientation within 3D space when evaluating the behaviour of soil under certain realistic stress paths.
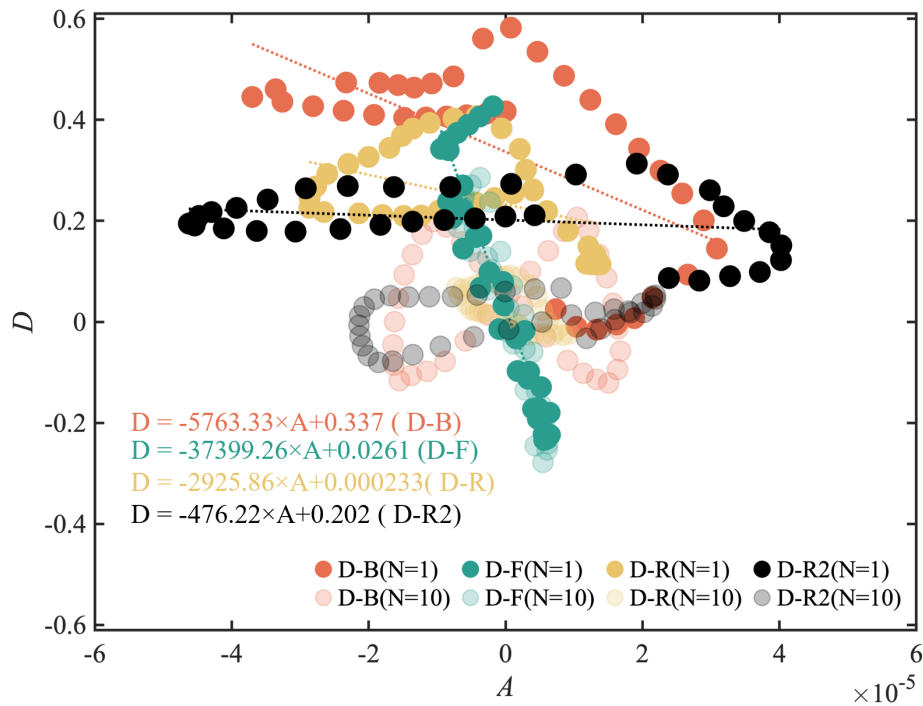
The observations made in this study are from a limited set of DEM numerical tests and do not exhaustively assess all possible influence factors, like mean stress, void ratio and particle shape, which warrant more in-depth investigations.

Conflicts of Interest

The authors declare no conflicts of interest. The complete review history is available online.

References

Arthur, J. R. F., del C., J. I. R., Dunstan, T., and Chua, K. S. (1980). Principal stress rotation: A missing parameter. *Journal of the Geotechnical Engineering Division*, 106(4):419–433.

Bagi, K. (1996). Stress and strain in granular assemblies. *Mechanics of Materials*, 22(3):165–177.

Open Geomechanics, 2022, article no. 4

Zhan He, Long Xue, Rui Wang & Jian-Min Zhang, *Response of granular material under combined principal stress value and orientation change in 3D space*

13

Figure 13. Scatter plot of dilatancy versus A at 1st, 10th cycle of the seismic load simulation stress paths tests D-B, D-F, D-R, D-R2. The linear fit between dilatancy D and the initial fabric anisotropy variable A for the first load cycle is also plotted for reference.

Bian, X., Li, W., Qian, Y., and Tutumluer, E. (2020). Analysing the effect of principal stress rotation on railway track settlement by discrete element method. *Géotechnique*, 70(9):803–821.

Cundall, P. A. and Strack, O. D. L. (1979). A discrete numerical model for granular assemblies. *Géotechnique*, 29(1):47–65.

Fu, P. and Dafalias, Y. F. (2012). Quantification of large and localized deformation in granular materials. *International Journal of Solids and Structures*, 49(13):1741–1752.

Gu, X., You, Z., Qian, J., and Li, W. (2020). The deformation of granular materials under repeated traffic load by discrete element modelling. *European Journal of Environmental and Civil Engineering*, 24(8):1135–1160.

Guo, N., Yang, F., Yang, Z., and Zhao, S. (2022). Deformation characteristics of inherently anisotropic granular media under repeated traffic loading: a dem study. *Acta Geotechnica*, pages 1–19.

Ishihara, K. and Towhata, I. (1983). Sand response to cyclic rotation of principal stress directions as induced by wave loads. *Soils and Foundations*, 23(4):11–26.

Ishihara, K. and Yamazaki, A. (1984). Analysis of wave-induced liquefaction in seabed deposits of sand. *Soils and Foundations*, 24(3):85–100.

Ishihara, K. and Yamazaki, F. (1980). Cyclic simple shear tests on saturated sand in multi-directional loading. *Soils and Foundations*, 20(1):45–59.

Itasca, C. (2018). Pfc 3d-user manual. *Itasca Consulting Group*, page 435.

Jiang, M., Shen, Z., and Sun, R. (2020). Dem analysis of undrained cyclic simple shear test on saturated sand. *Japanese Geotechnical Society Special Publication*, 8(12):485–488.

Li, X. (1997). Rotational shear effects on ground earthquake response. *Soil Dynamics and Earthquake Engineering*, 16(1):9–19.

Li, X., Yang, D., and Yu, H.-S. (2016). Macro deformation and micro structure of 3d granular assemblies subjected to rotation of principal stress axes. *Granular Matter*, 18(3):1–20.

LI, X. and YU, H.-S. (2010). Numerical investigation of granular material behaviour under rotational shear. *Géotechnique*, 60(5):381–394.

Miura, K., Miura, S., and Toki, S. (1986a). Deformation behavior of anisotropic dense sand under principal stress axes rotation. *Soils and Foundations*, 26(1):36–52.

Miura, K., Toki, S., and Miura, S. (1986b). Deformation prediction for anisotropic sand during the rotation of principal stress axes. *Soils and Foundations*, 26(3):42–56.

Nakata, Y., Hyodo, M., Murata, H., and Yasufuku, N. (1998). Flow deformation of sands subjected to principal stress rotation. *Soils and Foundations*, 38(2):115–128.

Satake, M. (1982). Fabric tensor in granular materials. In *IUTAM Conference on Deformation and Flow of Granular Materials, 1982*, pages 63–68. AA Balkema.

Sibille, L., Villard, P., Darve, F., and Aboul Hosn, R. (2019). Quantitative prediction of discrete element models on complex loading paths. *International Journal for Numerical and Analytical Methods in Geomechanics*, 43(5):858–887.

Tong, Z., Fu, P., Dafalias, Y. F., and Yao, Y. (2014). Discrete element method analysis of non-coaxial flow under rotational shear. *International Journal for Numerical and Analytical Methods in Geomechanics*, 38(14):1519–1540.

Towhata, I. and Ishihara, K. (1985). Undrained strength of sand undergoing cyclic rotation of principal stress axes. *Soils and Foundations*, 25(2):135–147.

Wang, R., Cao, W., and Zhang, J.-M. (2019a). Dependency of dilatancy ratio on fabric anisotropy in granular materials. *Journal of Engineering Mechanics*, 145(10):04019076.

Wang, R., Fu, P., Zhang, J.-M., and Dafalias, Y. F. (2019b). Deformation of granular material under continuous rotation of stress principal axes. *International Journal of Geomechanics*, 19(4):04019017.

Wichtmann, T. and Knittel, L. (2020). Behaviour of granular soils under uni- and multidimensional drained high-cyclic loading. In Triantafyllidis, T., editor, *Recent Developments of Soil Mechanics and Geotechnics in Theory and Practice*, pages 136–165, Cham. Springer International Publishing.

Wu, Q., Yan, L., and Yang, Z. (2021). Discrete element simulations of drained granular material response under multidirectional rotational shear. *Computers and Geotechnics*, 139:104375.

Xue, L., Kruyt, N. P., Wang, R., and Zhang, J.-M. (2019). 3d dem simulation of principal stress rotation in different planes of cross-anisotropic granular materials. *International Journal for Numerical and Analytical Methods in Geomechanics*, 43(14):2227–2250.

Yang, Z. X., Li, X. S., and Yang, J. (2007). Undrained anisotropy and rotational shear in granular soil. *Géotechnique*, 57(4):371–384.

Zeghal, M., El-Shafee, O., and Abdoun, T. (2018). Analysis of soil liquefaction using centrifuge tests of a site subjected to biaxial shaking. *Soil Dynamics and Earthquake Engineering*, 114:229–241.

Open Geomechanics, 2022, article no. 4
Zhan He, Long Xue, Rui Wang & Jian-Min Zhang, *Response of granular material under combined principal stress value and orientation change in 3D space*

15